Supernova Neutrinos in Liquid Argon TPCs

Candidate 107754

May 17, 2017

Supervisor: Dr Simon Peeters

Word Count: 11736

Abstract

Liquid argon time projection chambers can detect neutrinos, and for the purpose of this project will be simulated to detect supernova neutrinos with a threshold energy of 5 MeV. Initially using two fluxes within a SNOwGLoBES simulation with three different detector configurations the total smeared event rates for GVKM flux were 916, 1558 and 3672 and for Livermore flux were 807, 1376, 3243 (for 10, 17 and 40 ktonne respectively). For a supernova that could occur in the large magellanic cloud, just like SN1987A, a liquid argon detector of 10, 17 and 40 ktonne volumes could potentially achieve 30±10 , 65±15 and 150±50 events respectively. Whilst SNOwGLoBES employs a 17 ktonne detector as standard, a 10 ktonne and 40 ktonne have been added to simulate a DUNE-like detector consisting of a single module of 10 ktonne of active volume and four modules totalling 40 ktonne. From the results of these simulations it has been concluded that a liquid argon TPC as described could not confidently detect a supernova event from Andromeda due to statistical fluctuations in results, background rates and detector limitations.

Contents

1 Preface

The data used in the SNOwGLoBES simulation is included with the SNOwGloBES development version unless otherwise stated. I have used SNOwGLoBES 1.1 in my initial research, and then migrated to SNOwGLoBES 1.2 (development version) to obtain a time dependant Garching model. The manipulation and discussion of the inputs and outputs is my own work unless referenced otherwise. All plotting of graphs and creation of tables are entirely my own work unless referenced otherwise, codes are provided in the appendix. All graphs have been plotted in Python 2.7 [1] unless referenced otherwise. My conclusions are entirely my own work. Any materials such a graphs, conclusions and data that are not my own have been referenced accordingly.

2 Introduction

The required information on neutrinos, supernovae, detectors and SNOwGLoBES software will be described in this theory section. This will be focused mainly on liquid argon time projection chambers (TPCs) such as DUNE. SNOwGLoBES has been used to run simulations of a supernova at a distance of 10 kpc with active detector volumes of 10, 17 and 40 ktonne. Discussions into neutrino oscillations, background rates and distance have all been accounted for in final conclusions and have been described throughout where appropriate.

3 Neutrinos

3.1 A brief history

First postulated by Pauli in 1930, the neutrino could explain how beta decay could conserve energy spin and momentum [2]. The energy conservation of such a reaction was under question because using the models of the time would suggest electrons should be emitted with a discrete amount of energy rather than the continuous spectrum of energies observed. Initially named as a neutron to signify being a neutral particle, it was realised at this time that a particle this small would have challenges associated with detection. Fermi later suggest a name of neutrino (little neutral one) [3] which likened the particle to the neutral neutron, but smaller. The postulation of the neutrino explained why a continuous spectrum of beta decay particles were observed instead of a discrete energy state. Electrons are known to belong to discrete energy levels and therefore another particle must be the reason behind these continuous spectra observed. In 1956, Cowan and Reines observed antineutrinos from inverse beta decay occurring in water. This provided a blueprint for future detectors; a large body of liquid scintillator surrounded by photomultiplier tubes. The neutrinos detected by Cowan and Reines were anti-neutrinos produced from inverse beta decay. This process is commonly found in nuclear reactors and is shown below.

$$\overline{\nu}_e + p \rightarrow e^+ + n \tag{1}$$

In this interaction the electron antineutrino will interact with the proton and produce a neutron and positron. This positron will annihilate with an electron and produce detectable gamma rays [4].

3.2 Neutrino properties

Neutrinos are electrically neutral, spin half particles. There are three flavours of neutrino in the standard model: electron, muon and tau neutrino, all corresponding to the leptons [5]. The neutrinos all have constituent antiparticles which consist of the same characteristics except having opposing spin or helicity (z-component of spin). Neutrinos are considered to be left-handed whilst antineutrinos will be right-handed. Whilst being massive, there are considered to be two models of neutrino: Dirac and Majorana. Dirac neutrinos have neutrinos and antineutrinos being different particles, whilst Majorana neutrinos consider particle antiparticle duality [6]. In a more complex sense, Dirac neutrinos will require global symmetry whereas Majorana would be possible if lepton number symmetry was not conserved. Physicists have been able to calculate upper mass limits of neutrinos in various ways such as considering the neutrinos detected during the SN1987A event [7]. Each flavour of neutrino has a different flux expectation as discussed later. For the purpose of this report ν_x is defined as the sum $\nu_\tau + \overline{\nu}_\tau + \nu_\mu + \overline{\nu}_\mu$. Neutrinos can come from many different sources: the Sun, supernovae, nuclear fission and many more atmospheric and cosmological sources. Each of these sources has an almost unique signature in the form of flux and energy range as shown in Figure 1.

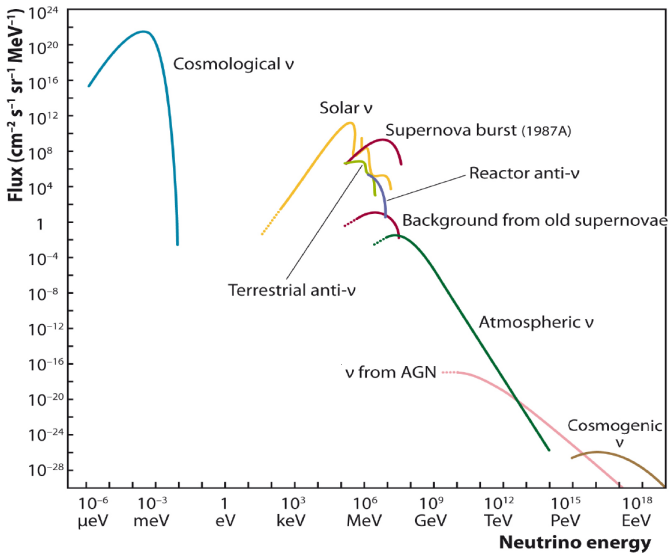

Figure 1: Neutrino fluxes against energy [8].

3.3 The solar neutrino problem

The solar neutrino problem describes how the number of electron neutrinos detected on Earth would not be the same as the expected amount predicted by the current solar model. Raymond Davis discussed the results of the Homestake and Kamiokande II experiment with reference to the expected solar flux. Davis concluded that approximately one third of neutrino events were accounted for from the Homestake experiment whilst around one half were accounted for with the Kamiokande II experiment [9]. The Homestake experiment was sensitive to electron neutrinos whilst the Kamiokande II experiment was less sensitive, but able to detect all flavours of neutrino from elastic scattering events. It is considered that the Sun will produce electron neutrinos whilst burning elements available in a star, and therefore a flux of purely electron neutrinos would be expected from solar model.

$$ {}^{1}_{1}H + {}^{1}_{1}H \rightarrow {}^{2}_{1}He + e^{-} + \nu_e \tag{2} $$

Further iterations of this reaction as the burning elements become heavier will still only produce one type of neutrino, the electron neutrino. The full electron neutrino flux was not observed, and therefore a theory of neutrino oscillations was used to explain this phenomena.

3.4 Neutrino oscillations

Neutrino oscillations explain how neutrinos created with one particular lepton flavour can later be measured as being a different flavour and suggests how neutrino flavour ratios would vary from the expected results. When measuring the total number of neutrino flux from a source the total numbers would remain correct [10]. This idea is not implemented explicitly in the simulations run through SNOwGLoBES, but have been discussed briefly. Neutrino oscillations can have certain probabilities based on θ, length, energy and Δm.

$$ P(|\nu_\alpha\rangle \rightarrow |\nu_\beta\rangle) = sin^2(2\theta) sin^2\left(\frac{1.27\Delta m^2}{E/L}\right) \tag{3} $$

$$ \Delta m_{12} = m_1 - m_2 \tag{4} $$

This is a two flavour approximation which provides an idea of how neutrino oscillations are affected by distance and mass. Given that optimal oscillation lengths are in the order of thousands of kilometers (and then periodic) it would be difficult to calculate this effect accurately for a distance in kiloparsec. Neutrino oscillations will behave differently through space when compared to how they act when travelling through a dense medium such a the Sun and a supernova event [11]. The SNO observatory provided it's first conclusive results and data in 2001 [12] and provided an explanation to the missing solar neutrinos. " *We now have high confidence that the discrepancy is not caused by problems with the models of the Sun but by changes in the neutrinos themselves as they travel from the core of the Sun to the earth,*" said Dr. Art McDonald, SNO

Project Director and Professor of Physics at Queen's University in Kingston, Ontario [13].

4 Supernovae

4.1 Classification

Supernovae are theorized to occur in two different ways: they can be caused by thermonuclear explosions of stars in binary systems or by the core collapse of a massive star [14]. The core collapse of a massive star relies on the star having a mass greater than $8M_{\odot}$. Any stars lower than this mass are not guaranteed to have enough gravitational potential energy to complete every burning process up to iron, and would not be able to initiate a core-collapse. Supernovae can be classified based upon the presence of particular elemental spectral lines, and the mechanism under which they happen.

4.1.1 Type Ia

Type Ia supernova are observed in a binary system of stars and rely on a critical mass being reached (the Chandrasekhar mass), approximately $1.4M_{\odot}$. A white dwarf will accrete matter from the secondary star in the binary system until this mass limit is reached. Because of this known mass, type Ia supernovae can be used as standard candles for determining distances as the measured luminosities from known events have remained the same and therefore their observed magnitude only depends on distance from the observer [15].

4.1.2 Type Ib and Ic

Type Ib and Ic supernovae have no presence of hydrogen lines in their emission spectra, but are still considered to be core collapse supernovae. It is thought that the outer layers of the star have been removed by stellar winds whilst leaving a majority of the star unchanged. Type Ib have been stipped on their hydrogen, whilst Ic have been stripped of their hydrogen and helium. They can both be referred to as stripped core collapse supernovae [16].

4.1.3 Type II

Type II supernovae are also core collapse supernovae but have hydrogen lines present. Core collapse supernovae are a source of cosmic neutrinos as well as being one of the highest, most destructive power outputs in the known universe. Core collapse supernova are predicted to occur every 20-50 years within our galaxy [17]. For this simulation it will be assumed that we are observing a type II supernova for they are most consistently documented, whilst being the most frequent type of core-collapse supernova currently observed. Type II supernova can be further classified upon their spectral decay shape, although for this discussion will not be required.

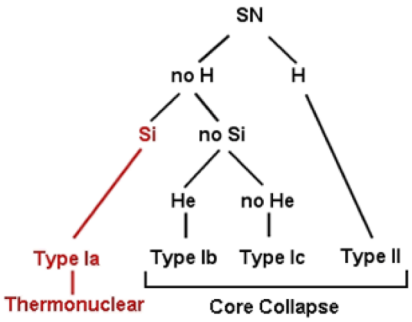

Figure 2: A supernova classification tree [18].

4.2 Main Sequence Lifetime

Aside from the formation of such a star, most of the lifetime of a star with mass above $8M_{\odot}$ will be spent cycling through various burning processes. Stars undergo burning processes whereby they will collapse under the gravity of their own material and will heat up due to the increase in pressure. This increase in temperature will eventually lead to a burning process of the lightest element available at the time until this fuel is exhausted. The hydrogen burning phase exists for tens of millions of years. Hydrogen burning provides a counterbalance to the core collapse but eventually the hydrogen fuel is exhausted. Once this has happened the star will begin to contract and heat up. If a sufficiently high enough temperature is reached the star will begin the helium burning process (note the helium was a byproduct of the hydrogen burning process). The star will swell at this point and will become large enough to classify as a red giant. Lower temperate fusion products will migrate towards the surface of the star in order of density forming an onion-like structure. Each burning process will produce less energy than the last, meaning they will hold gravitational collapse for less time. The final silicon burning process will last for a matter of days.

4.3 Supernovae

The burning processes will repeat (and speed up after each process exponentially) until the last fuel left is iron. Due to the stability of iron, a burning process will not occur and the outer layers of the star will collapse inwards. This collapse is halted by electron degeneracy pressure which will not allow electrons to occupy the same state in space. This quantum mechanical effect arises from Paulis exclusion principle which forbids fermions to occupy the same quantum mechanical state [20]. At this point the core collapse will halt as the density of the core will be comparable to an atomic nucleus. The infalling matter rebounds and produces a shockwave. Pre-collapse, high energy electrons which are withholding the collapse of the star can be captured by protons and

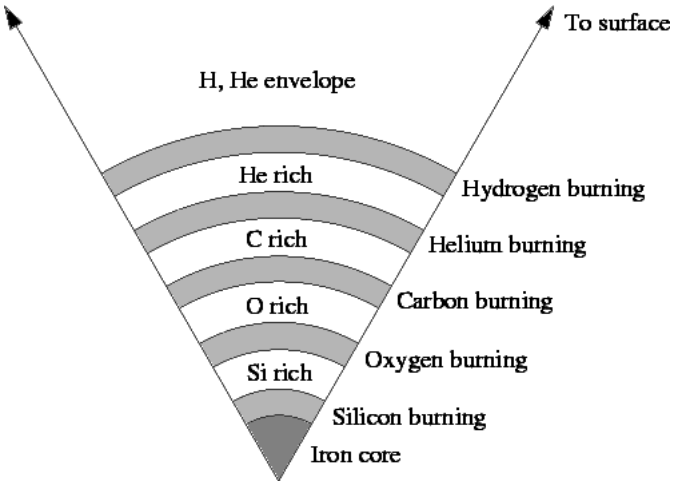

Figure 3: Onion-like structure of a star nearing the end of it's life [19].

the heavy nuclei of the core. In this inverse beta decay, the core would begin to contract at supersonic speeds leaving behind neutrinos which will propagate outwards. As the density increases in this scenario, the neutrinos will no longer be free to propagate outwards and will create a neutrino sphere which is defined as the region between where neutrinos are trapped and where they are free to propagate. The resulting shockwave of this supernova event will blow the outer layers of the resulting structure apart and therefore release the neutrino sphere. Post explosion, in the order of 1 second, the outer part of the supernova will settle and it's energy will be released in the form of neutrinos. The inner core will become an object in itself and left behind to cool by emitting antineutrinos of all flavours in a 5-10 second shell. One is left with various neutrino shells propagating through space which are in the order of 10 seconds thick with varying density. Post-supernova the remnant of the star may proceed to become a neutron star or a black hole. The supernova remnant can experience such high gravitational force that remaining protons and electrons can combine to become neutrons, thus the name neutron star. Neutron stars will experience a high rotational force from the supernova explosion, and the high density of the material will maintain this rotation [21]. Should a black hole form there would be an instant drop in the neutrino flux at the time where the graviational pull of such a dense object becomes too much for the resultant neutrinos and photons to escape from the event horizon.

5 Supernova Neutrinos

5.1 Motivation

Supernova neutrinos are a valuable source of information from the interior of a supernova. Supernovae provide an opportunity for further study of both neutrinos and supernovae. This opportunity, albeit rare, has sparked an interest from both particle physicists and astronomers alike. A particle from the interior of a supernova could provide information on the collapse mechanism of such an event. Approximately 99% of all energy released from a supernova explosion will be carried away by neutrinos under the current model. More neutrinos are produced during this supernova event than produced over the entire lifetime of the star [22]. Due to weak interactions, supernova neutrinos are ejected outwards quicker than photons from a supernova as photons are more likely to be absorbed and reemitted several times through a dense medium. This leads to a neutrino shell propagating through space and reaching the observer in the order of hours before visible light. This is the basis that the Supernova Early Warning System (SNEWS) is built upon. Supernova neutrinos can be detected hours before visible light and therefore provide a warning signal that visible light from a supernova is close behind. With supernovae being such rare events, it can be beneficial to run simulations prior to the event to ensure that certain limits are predetermined or estimated such as: maximum distance to supernova to be observable, expected number of events and statistical probabilities of coincidental events.

5.2 SN1987A

SN1987A was the first observation of neutrinos arriving at Earth from the supernova before photons. This suggests that the neutrinos must be travelling close to the speed of light otherwise the time difference between neutrinos and photons would be much more significant. If the neutrinos were travelling significantly slower than the speed of light, the distance from the supernova (in the order of 10-100 kpc) would allow for the photons released to catch up and overtake the neutrinos before they arrived at Earth. SN1987A occurred about 50 kpc away from Earth in the Large Magellanic Cloud. Neutrinos were detected at 3 different detectors worldwide. Kamiokande detected 12 antineutrinos [23], IMB detected 8 antineutrinos [24] and Baksan detected 5 neutrinos [25]. These events were detected within ranges of 13, 6 and 9 seconds respectively. It has been discovered that most of the events occured within a few seconds of the first signals being detected, with a few more events occuring towards the later end of the detection [26].

5.3 SNEWS

SNEWS collaborates with numerous detectors worldwide to allow for a system where early warning signs of a supernova (in particular the neutrinos arriving

in the order of hours earlier than the light) can be used as a warning that a supernova event has happened and visible light will be on its way. The level of collaboration between experiments will allow for a reliable signal, and will also help to better understand signal sensitivities of current and future experiments. The warning system requires an alert to fill three main criteria where possible: prompt, pointing and positive. Prompt is defined as having a minimal delay in the signal time from the neutrino detections - and is suggested that a delay of minutes would be expected from such an automated system. Pointing allows the direction of the supernova to be determined. Certain detection techniques can provide a directional signal but if this is not available a direction can be figured out from triangulation of several different signals worldwide. Positive means that the signal has to be certain to ensure that false signals aren't sent out to such a large network. They have provided an acceptable number of one false alert per century. If two different detectors send a signal within ten seconds of each other it is assumed that any system faults or statistical anomalies could be ruled out as they would be unlikely to occur at the same time at two different sites [27]. The more detectors involved with the SNEWS collaboration will allow for further reduction of false signal as well as reducing the effects of statistical errors, detector errors and routine maintenance of detectors. Having a signal to predict when a supernova may happen could provide invaluable information to the astrophysical community as these rare events will have a much greater chance of high quality and frequent observations when predicted successfully.

6 Neutrino Detectors

6.1 Neutrino Detection techniques

6.1.1 Cherenkov radiation

When a particle travels through a medium faster than the speed of light in said medium, a cone of Cherenkov light will be radiated. This cone is directional and therefore can be used to recreate the direction of the incoming particle. A water Cherenkov detector will use photomultiplier tubes to detect a circular projection of this cone of light. Particles, such as electrons, will scatter during this process and will produce a lower quality signal. When measuring this light, the cone will appear as a ring of light detected by the photomultiplier tubes. This ring of light will appear fuzzy if scattering occurs. Cherenkov detectors have a detection threshold in the order of a few MeV which is considered to be high when detecting neutrinos.

6.1.2 Scintillation

Scintillation is a chemical process of luminescence where light of a characteristic spectrum is emitted following the absorption of radiation. Scintillation light measurement is not affected by direction and is isotropic. This means that on its own, scintillation light does not allow for reconstruction of particle direction [28]. There is a generally low energy threshold (lower than water Cherenkov) which means that particles of lower energies can be detected. This can be beneficial to obtain a wider spectrum of neutrino energies, whilst allowing background rates of lower energy to have a higher impact on results. In liquid argon there are two notable scintillation processes: self trapped exciton luminescense and recombination luminscense. In the first process an argon atom is excited from a collision which will in turn become paired with another argon atom. This eximer will decay releasing photons for detection. In the second process, an argon atom is ionized from a collision which will then become paired with another argon atom and will form another eximer with another electron. This eximer will once again emit photons which can be detected [29]. Both of these processes rely on an eximer state of two atoms being bound together in a low energy state. These states can either be a singlet or triplet state which has an impact on the decay time. This singlet or triplet state depends on how the electron spin combines with the two bound argon atoms. Singlet decay times are approximately 6 ns whilst triplet decay times are approximately 1500 ns [30].

6.2 Detectors

6.2.1 Water Cherenkov Detectors

An example of a water Cherenkov neutrino detector is Super Kamiokande. It consists of 50 ktonne of ultra pure water and is surrounded by over 11,000

photomultiplier tubes. Being situated one kilometre underground reduces background rates of detection, limiting it to only high energy muons and neutrinos produced from cosmic ray showers [31]. The SNO detector is another example of a water Cherenkov detector. It consisted of 1 ktonne of heavy water and was sensitive to charged current, neutral current and elastic scattering interactions. In the neutral current interaction, the neutrino would cause the deuteron to split into it's constituent proton and neutron. The neutron will be captured with a deuteron and will radiate a photon with energy approximately 6 MeV. This interaction will be sensitive to all neutrino flavours.

$$\nu_x + d \rightarrow n + p + \nu_x \tag{5}$$

In the charged current interaction the neutrino will produce another proton from the neutron in the deuteron. An electron is produced as a byproduct of this interaction and will be detected with energies in the order of 10 MeV. This interaction will be sensitive to only electron neutrinos.

$$\nu_e + d \rightarrow e^- + p + p \tag{6}$$

Elastic scattering interactions will operate in the same way that Super Kamiokande detects neutrinos and whilst will be dominated by electron neutrinos will technically be sensitive to all three flavours [32].

$$\nu_x + e^- \rightarrow \nu_x + e^- \tag{7}$$

6.2.2 Liquid Scintillator Detectors

Following a similar approach, scintillators require a large, enclosed volume of target material surrounded by photo sensors. Scintillator detectors are capable of having a lower energy threshold than water Cherenkov detectors. An example in progress will be the SNO+ detector [33]. The SNO+ detector is the next stage of what was the SNO detector. SNO+ will exist in several different phases: a water Cherenkov stage to allow for calibration and eventually having a fully loaded scintillator stage in the search for neutrino-less double beta decay [34]. This would help determine whether the Majorana or Dirac model is correct. If neutrino-less double decay is observed then a neutrino and antineutrino could be considered the same particle just in a different reference frame. The search for neutrinoless double beta decay will ultimately use ^{130}Te, although will initially be using linear alkylbenzene (LAB) as a solvent. The tellurium could then be dissolved efficiently in the liquid scintillator whilst still maintaining the optical properties desired for such an experiment. The SNO+ detector will be situated just over two kilometers underground to reduce effects of backgrounds such as cosmic muons [35].

6.2.3 Liquid Argon Detectors

Liquid argon time projection chambers provide a three dimensional reconstruction of a charged particle track created from a neutrino interaction. A flash of

scintillation light will provide a start time for the interaction. A liquid argon time projection chamber consists of a large volume of liquid argon. Liquid argon condenses at -186^oC which means it can be condensed using liquid nitrogen (which has a boiling point of -196^oC) from the air. This is possible because argon has a boiling point between oxygen and nitrogen, so it is possible to use these temperature differences to separate the gasses [36]. When condensing from the air, it becomes relevant that nitrogen will quench scintillation light and oxygen will trap free electrons. Both of these impurities would directly impact the effectiveness of such a detector. Purity of the liquid argon is key to obtaining the optimum number of detections during a supernova event. The ICARUS collaboration submitted a research paper in 1993 [37] with a design for a fully tested liquid argon purifier. The liquid argon would be evaporated and passed through Oxisorb cartridges [38] and a molecular sieve to ensure that even in the prescence of water vapour a maximum amount of oxygen is removed from the gas. A nitrogen trap also features as part of the design. It is quoted that a purity of 0.1 ppb O_2 is obtained.

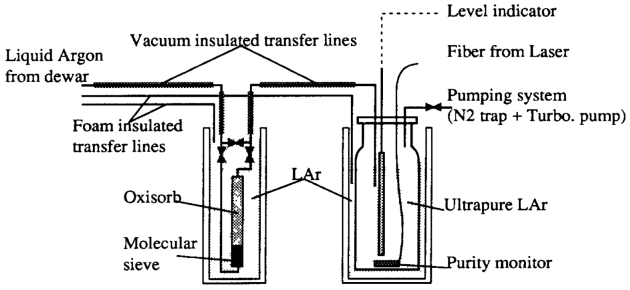

Figure 4: A schematic showing a liquid argon purification system [37] .

Fermilab later suggested a design of a LAPD (Liquid Argon Purity Demonstrator) which could show how to purify liquid argon without the need to evacuate the cryogens where the argon would be for experimental purposes. The first stage of purification requires the containment vessel to be purged with argon gas. After this first step the gas will be heated slightly to dry the volume of the container. The next stage requires the liquid argon to be passed through filters (including a molecular sieve) multiple times until a purification of 1 ppb is achieved. This is more cost effective than purification outside of the experiment [39]. When a neutrino interacts with the liquid argon it ionises and excites the argon and upon recombination, scintillation light will be emitted. An array of photomultiplier tubes (coated in wavelength shifting material in the ICARUS detector [40]) would detect the scintillation light. Liquid argon is transparent to its own scintillation light as the luminescent peaks at 128 nm which would not provide enough energy for secondary ionization. This adds to the desirability of liquid argon as a detection medium. Byproducts from this interaction would include a charged lepton along with either a neutron or proton which will pass through the liquid argon, knocking electrons free from

the argon. These electrons will flow towards the back of the detector and will leave a characteristic trail of particular interactions. There are three planes of wires in a liquid argon neutrino detector: two will create an inductive pulse as the charge passes through and a third and final plane will collect this charge. These three dimensions of planes allow three dimensional reconstruction of the particle tracks. Pointing would not be possible from charged current neutrino interactions in liquid argon. It would be possible to attempt a reconstruction of direction from elastic interactions as the electrons produced from such an interaction would show an average direction which would be approximately in the direction of the travelling neutrino. In the same sense, it would be possible to rule out directions that the electrons have not pointed in. From this information it would be possible to recreate directions to look for the supernova (much more so than having no pointing), but with limited accuracy. This pointing information would become even more valuable in collaboration with other neutrino detectors.

DUNE (Deep Underground Neutrino Experiment) has been simulated in this research for the purpose of being a supernova neutrino detector. DUNE [41] will have four cryogens containing 17 ktonne of liquid argon with an active volume of 10 ktonne per cryogen. Whilst it is not it's primary purpose, DUNE is capable of detecting supernova neutrinos should such an event happen. A beam of neutrinos will be fired from Fermilab and will be detected by a near and far detector with the aim of measuring neutrino oscillations over a 1300 km distance. Having a detector at either end of this distance will allow for accurate reconstruction of flavour ratio before and after the neutrinos has travelled through the Earth. This distance is in the correct order to maximize neutrino oscillation probability. The experiment also aims to determine the mass hierarchy of the three proposed neutrino flavours more accurately. The experiment will be built one module at a time, allowing for an initial 10 ktonne detector to be up and running before the rest of the experiment.

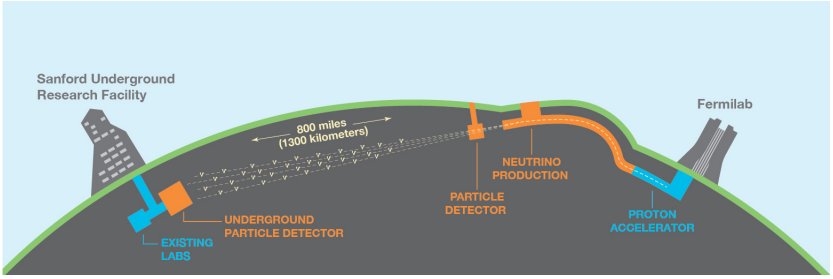

Figure 5: A diagram of DUNE [42] .

7 SNOwGLoBES

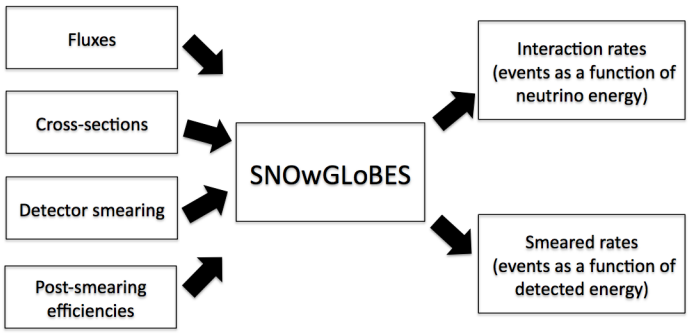

Figure 6: SNOwGLoBES schematic indicating the four main inputs and two outputs for a given detector configuration and fluence [43].

SNOwGLoBES [43] is a software that runs using GLoBES [44] and will provide two different outputs of events as a function of neutrino energy and events as a function of detected energy. The inputs include: detector configuration (which consists of the material used and the size), fluences, and smearing matrices.

7.1 Fluences

In SNOwGLoBES 1.1 there are two different models of fluence built in. These are the GVKM [45] and Livermore [46] fluences. In SNOwGLoBES 1.2 a third, Garching flux model with time dependance is included.

7.1.1 Livermore

The Livermore fluence shows three distinct peaks and also having ν_e and $\overline{\nu}_e$ showing ratios of peak luminosity approximately 2:1. This fluence was produced from Monte Carlo simulations of results from the Super Kamiokande detector. The model is built on an optimum distance of 10 kpc. This model shows no time dependance as it has been integrated over 14 seconds to provide total event rates upon simulation. There appears to be no evidence of flavour conversion from this fluence as all of the neutrino flavours experience a smooth continous curve.

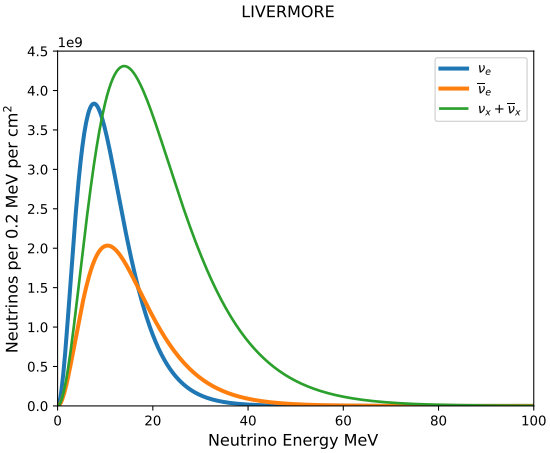

Figure 7: The Livermore fluence.

7.1.2 GVKM

The GVKM group fluence differs from the Livermore fluence as it approximates ν_e and $\overline{\nu}_e$ having similar peaks in luminosity. Electron neutrinos show an individual peak between 5 MeV and 10 MeV which illustrates the point where the infall of the supernova halts and neutrinization occurs. At this point the neutrinos flavours will vary from the original electron neutrinos being produced and give way to a wide spectrum of flavours and energies being produced. This is known as flavour conversion and happens whilst the other neutrino flavours are close to peaking due to some of the large amount of electron neutrinos. This model shows no time dependance as it has been integrate over 10 seconds to provide total event rates upon simulation.

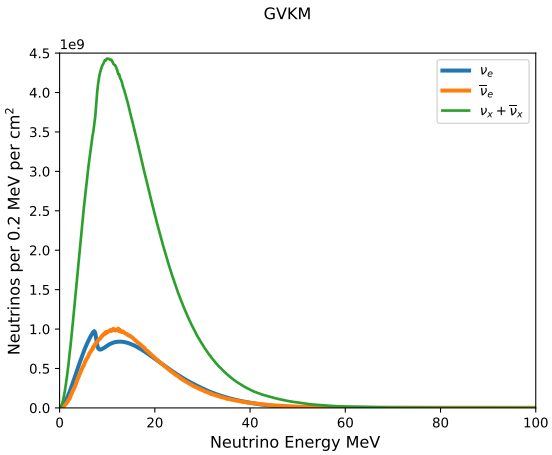

Figure 8: The GVKM fluence.

7.2 Neutrino interaction cross-sections

Cross sections for neutrino interactions in liquid argon are provided within SNOwGLoBES and are referenced from [47] and [48]. Figure 9 illustrates the charged current interactions alongside elastic scattering interactions. The coloured lines represent both charged current interactions and the black lines show elastic scattering interaction. This graph demonstrates that the anti electron neutrino interaction with argon have a cross section of zero from any neutrino energy below approximately 15 MeV. Up until this point the two cross sections show similarly decreasing gradients of cross section against Neutrino energy. Neutral current interactions are not considered in the SNOwGLoBES simulation "*due to lack of information in the literature about resulting observable products*" [43]. Charged current interactions (equations (8) and (9)) are sensitive to only electron neutrinos, whilst elastic scattering interactions (equation (10)) are sensitive to all neutrino flavours. Neutral current interactions would also be sensitive to all neutrino flavours.

$$\nu_e + {}^{40}Ar \rightarrow e^- + {}^{40}K^* \tag{8}$$

$$\overline{\nu}_e + {}^{40}Ar \rightarrow e^+ + {}^{40}Cl^* \tag{9}$$

$$e^- + \nu_x \rightarrow e^- + \nu_x \tag{10}$$

7.3 Detector configurations

There is one liquid argon detector pre-configured in this distribution and is described as AR17KT, a 17 ktonne detector. For comparison, a 10 ktonne (AR10KT) and 40 ktonne (AR40KT) detector have been added. The output of

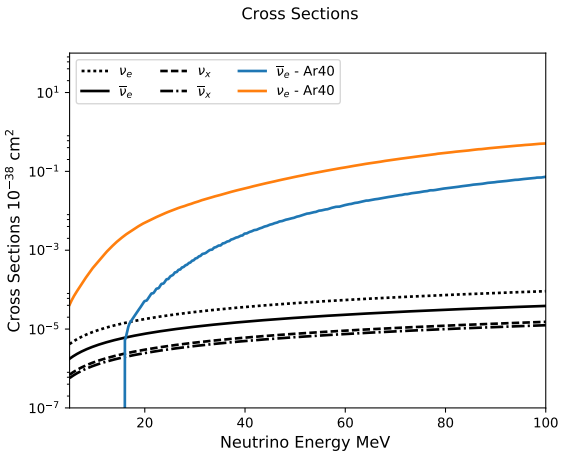

Figure 9: Cross sections of neutrino interactions in liquid argon.

SNOwGLoBES consists of two different event rates: events per 0.5 MeV against neutrino energy and events per 0.5 MeV against detected energy. The latter is referred to as the smeared rate and is provided by processing the output data through smearing matrices preconfigured in SNOwGLoBES. The smeared eventrate is what would be observed in a real detector as the initial neutrino energy would not be directly detected. Whilst the underlying software GLoBES can, SNOwGLoBES does not apply neutrino oscillation probabilities in its current build. The 10 ktonne and 40 ktonne detector configurations will demonstrate the expected event rates of a supernova at distance of 10 kpc in a single module, and all four modules of DUNE.

8 Simulation Results

8.1 10 ktonne

Simulations of a 10 ktonne liquid argon TPC have been run with both the GVKM and Livermore fluence models. A 10 ktonne detector will be equivalent to a single module of the DUNE detector.

8.1.1 Livermore

The Livermore fluence run with a 10 ktonne detector yielded a total of 862 events unsmeared and 807 events smeared. There is a peak in activity around 20 MeV for the total number of neutrinos. Elastic scattering neutrinos will constantly decrease with a higher energy. It is clear from the total interactions that electron neutrinos dominate the eventrate.

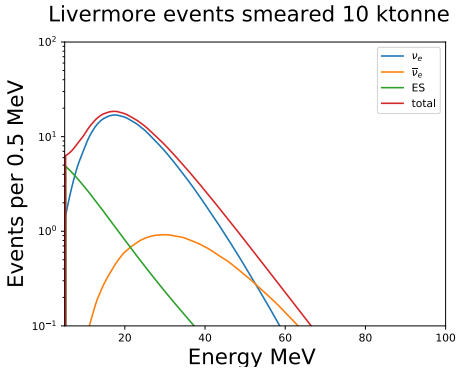

Figure 10: A plot of Events against neutrino energy for a 10 ktonne Liquid Argon TPC with the Livermore fluence.

Event	Events Livermore 10 ktonne Smeared
$\nu_e + {}^{40}Ar \rightarrow e^- + {}^{40}K^*$	669
$\overline{\nu}_e + {}^{40}Ar \rightarrow e^+ + {}^{40}Cl^*$	56
$\nu_x + e^- \rightarrow \nu_x + e^-$	82
Total	807

8.1.2 GVKM

The GVKM fluence run with a 10 ktonne detector yielded a total of 942 events unsmeared and 916 events smeared. In comparison the the Livermore fluence we see a much larger range of energies (ranging up to over 80 MeV for ν_e). $\overline{\nu}_e$ are comparably close the the Livermore eventrate with a peak just before 40 MeV and a relatively even distribution either side of the peak.

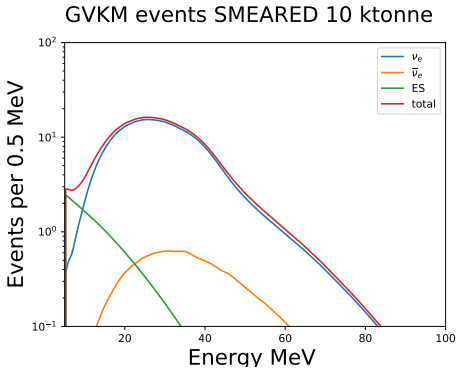

Figure 11: A plot of Events against neutrino energy for a 10 ktonne Liquid Argon TPC with the GVKM fluence.

Event	Events GVKM 10 ktonne Smeared
$\nu_e + {}^{40}Ar \rightarrow e^- + {}^{40}K^*$	828
$\overline{\nu}_e + {}^{40}Ar \rightarrow e^+ + {}^{40}Cl^*$	39
$\nu_x + e^- \rightarrow \nu_x + e^-$	49
Total	916

8.2 17 ktonne

Simulations of a 17 ktonne liquid argon TPC have been run with both the GVKM and Livermore fluence models.

8.2.1 Livermore

The Livermore fluence run with a 17 ktonne detector yielded a total of 1467 events unsmeared and 1376 events smeared. The larger detector has provided not only more events, but a wider range over energies. The range has increased by approximately 5 MeV for the Livermore fluence by increasing the mass of the detector by 7 ktonne. Because these higher energy neutrinos would have such a low event rate, it relies on having a larger detector to statistically capture these events.

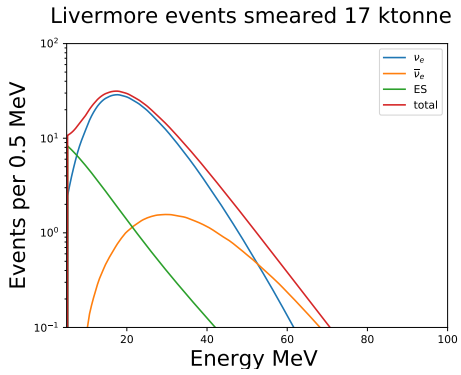

Figure 12: A plot of Events against neutrino energy for a 17 ktonne Liquid Argon TPC with the Livermore fluence.

Event	Events Livermore 17 ktonne Smeared
$\nu_e + {}^{40}Ar \rightarrow e^- + {}^{40}K^*$	1138
$\overline{\nu}_e + {}^{40}Ar \rightarrow e^+ + {}^{40}Cl^*$	95
$\nu_x + e^- \rightarrow \nu_x + e^-$	143
Total	1376

8.2.2 GVKM

The GVKM fluence run with a 17 ktonne detector yielded a total of 1601 events unsmeared and 1558 events smeared. Similarly to the Livermore fluence the

range of energies is even wider when considering a 17 ktonne detector with the GVKM fluence.

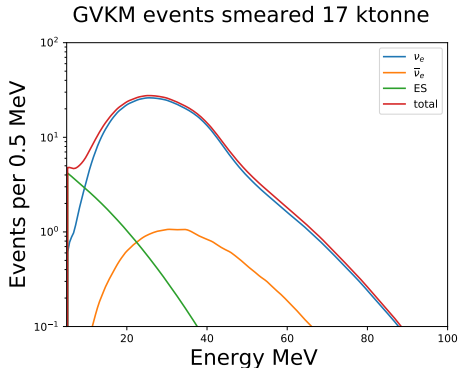

Figure 13: A plot of Events against neutrino energy for a 17 ktonne Liquid Argon TPC with the GVKM fluence.

Event	Events GVKM 17 ktonne Smeared
$\nu_e + {}^{40}Ar \rightarrow e^- + {}^{40}K^*$	1407
$\overline{\nu}_e + {}^{40}Ar \rightarrow e^+ + {}^{40}Cl^*$	66
$\nu_x + e^- \rightarrow \nu_x + e^-$	85
Total	1558

8.3 40 ktonne

Simulations of a 40 ktonne liquid argon TPC have been run with both the GVKM and Livermore fluence models. The results of these two simulations further demonstrate the effect of a detector with a larger active volume. A wider neutrino energy range, and a greater number of events.

8.3.1 Livermore

The Livermore fluence run with a 40 ktonne detector yielded a total of 3459 events unsmeared and 3243 events smeared.

Event	Events Livermore 40 ktonne Smeared
$\nu_e + {}^{40}Ar \rightarrow e^- + {}^{40}K^*$	2678
$\overline{\nu}_e + {}^{40}Ar \rightarrow e^+ + {}^{40}Cl^*$	225
$\nu_x + e^- \rightarrow \nu_x + e^-$	340
Total	3243

8.3.2 GVKM

The GVKM fluence run with a 40 ktonne detector yielded a total of 3778 events unsmeared and 3672 events smeared.

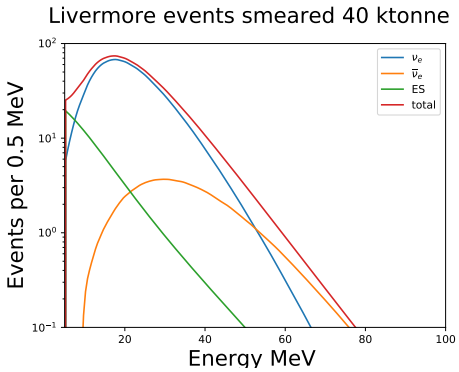

Figure 14: A plot of Events against neutrino energy for a 40 ktonne Liquid Argon TPC with the Livermore fluence.

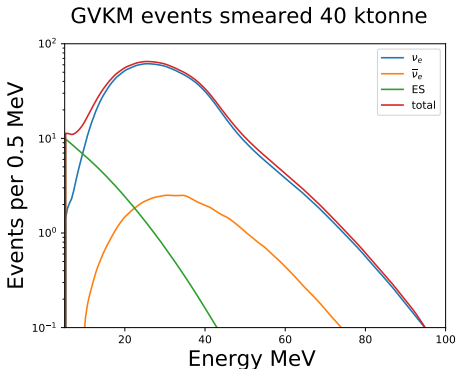

Figure 15: A plot of Events against neutrino energy for a 40 ktonne Liquid Argon TPC with the GVKM fluence.

Event	Events GVKM 40 ktonne Smeared
$\nu_e + {}^{40}Ar \rightarrow e^- + {}^{40}K^*$	3312
$\overline{\nu}_e + {}^{40}Ar \rightarrow e^+ + {}^{40}Cl^*$	156
$\nu_x + e^- \rightarrow \nu_x + e^-$	204
Total	3672

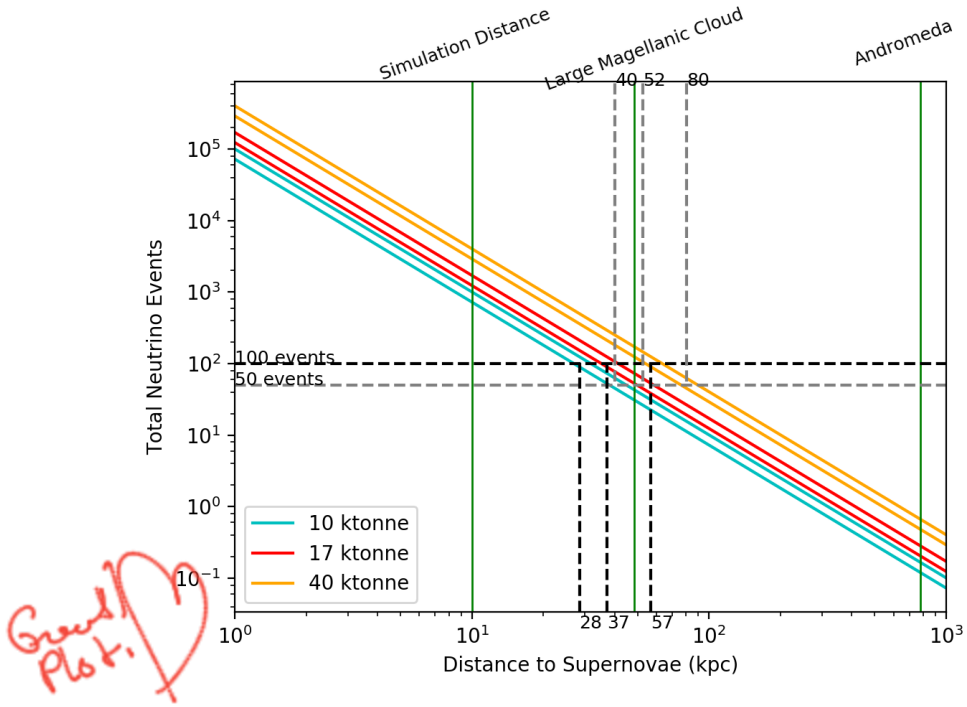

Figure 16: Plot of ~~distance~~ events against distance.

8.4 Distance

Neutrinos are ejected outwards into space in a spherical shell. Because of the nature of this $1/R^2$ dependance we can determine different rates of detection for supernovae that are a specific distance away. SNoWGLoBES builds in a distance of 10 kpc but using this proportionality a graph of distance against events has been obtained for the three different detector configurations. The different values of each detector type have used the Livermore and GVKM fluences as lower and upper bounds, with a 10% error each way. This graph shows that if 50 events were observed in these simulations, the 10, 17 and 40 ktonne detectors would determine the supernova occured as a distance of 40, 52 and 80 kpc respectively. The 40 ktonne detector would detect approximately one event from Andromeda. This means that a larger detector would detect more events from such a distance, but due to the errors and backgrounds involved with such a large detector it could not confidently detect a supernova from Andromeda.

From [49] one finds that an estimated optimum distance for supernova probability is approximately 15 kpc which would provide a total eventrate of 1750±250 events from a DUNE-like detector. Assuming a gaussian distribution of events against energy one could assume that a σ value equal to the standard deviation

divided by the square root of the number of interactions.

$$\sigma_\nu = \frac{\sigma}{\sqrt{N}} \tag{11}$$

Using this relation and considering that the number of events have a direct $1/R^2$ relation it could be concluded that the error on σ_ν will be proportional to the standard deviation multiplied by R.

$$\sigma_\nu \propto \frac{\sigma}{1/R} \propto \sigma R \tag{12}$$

For the 10 ktonne detector at distance 10 kpc with the GVKM fluence $\sigma = 5.56$ and $N = 918$ showing that $\sigma_\nu = 0.18$. Increasing this distance to 100 kpc yields $\sigma = 0.056$ and $N = 9$ showing that $\sigma_\nu = 0.018$. For the 40 ktonne detector at distance 10 kpc with the GVKM fluence $\sigma = 22.2$ and $N = 3675$ showing that $\sigma_\nu = 0.37$. Increasing this distance to 100 kpc yields $\sigma = 0.22$ and $N = 37$ showing that $\sigma_\nu = 0.037$. Taking into account that σ has it's own proportionality of $1/R^2$ we can conclude that

$$\sigma_\nu \propto \frac{1}{R} \tag{13}$$

As the distance to a supernova increases, it's number of interactions within the detector will decrease by R^2 and the error will decrease by R.

8.5 Garching Flux

The Garching flux model [50] used has been developed by running a Monte Carlo simulation to determine values for average energy and α to allow a calculation of flux for each of these values using the following relation.

$$f(E) \propto E^\alpha e^{-(\alpha+1)\frac{E}{\overline{E}}} \tag{14}$$

Using the development version of SNOwGLoBES and the ROOT [51] macros included, a plot of Garching luminosity, α, average neutrino energy and events against logarithmic time have been plotted. The macros for this plot are provided in the SNoWGLoBES development package [43]. From this plot it becomes obvious that just like the solar neutrino model, only electron neutrinos are created until the neutronization section of the supernova. During the neutronization, all flavour types are created and by the end of the neutronization section they are almost experiencing the same luminosity for each flavour. During the cooling period we experience a secondary peak of events at approximately two seconds. This explains how neutrino detectors see so many events before the first second is over, but will experience more events even up to, and beyond ten seconds.

It is possible to run the Garching flux over 300 time bins and use the data to determine a time dependant event rate. Once the simulation has been run over all time bins the data was plotted as follows: These plots show the rate of ν_e

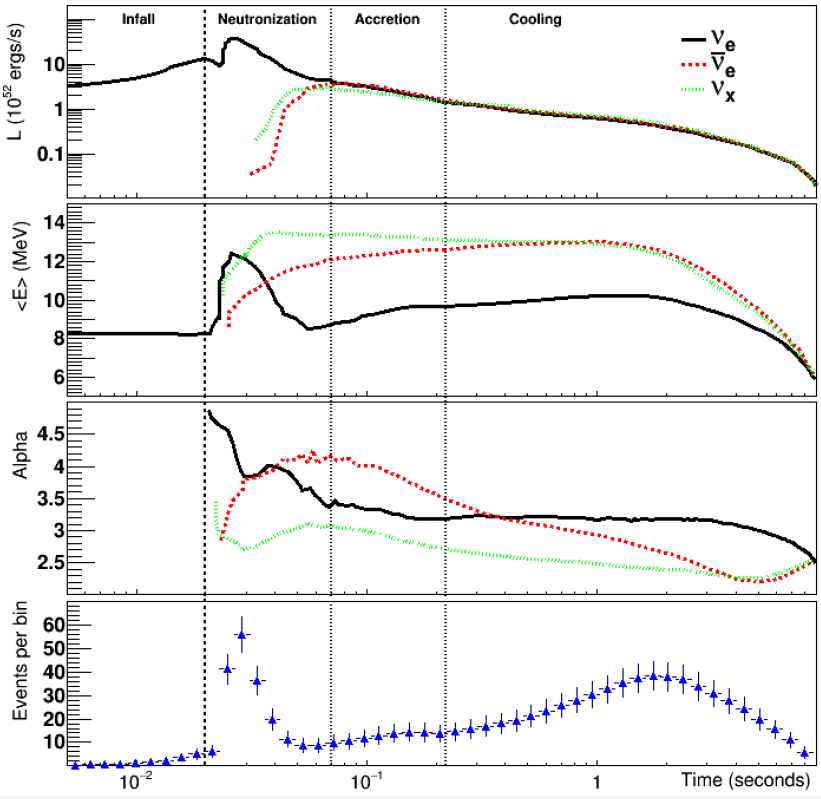

Figure 17: Plot of Garching flux from SNOwGLoBES development version. It includes luminosity, average neutrino energy, α, and events per bin all as functions of time.

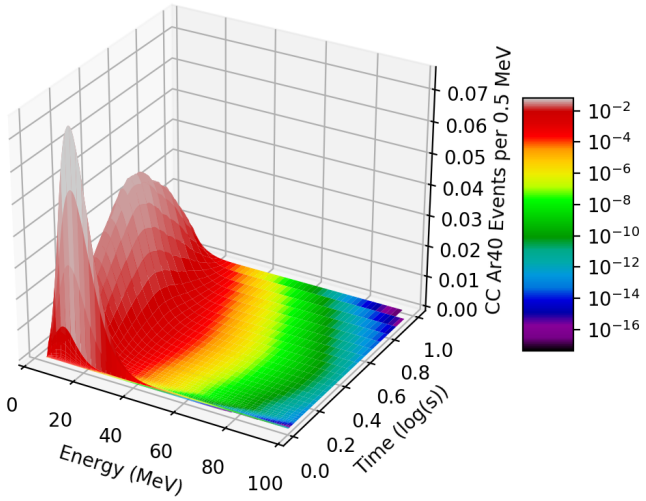

Figure 18: A three dimensional plot including detected energy, event rates per 0.5 MeV and logarithmic time.

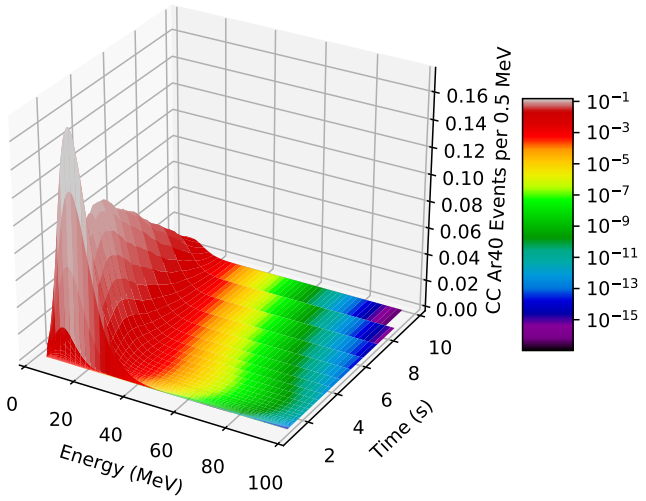

Figure 19: A three dimensional plot including detected energy, event rates per 0.5 MeV and time.

detection in a 17 ktonne liquid argon TPC. The first peak shows an initial burst of neutrinos which is halted as the neutrino sphere builds up in the interior of the supernova. This is known as the neutronization period. The second, more gradual, peak shows the release of this neutrino sphere with a similar range of energies but over a longer release time. This is known as the cooling period. The lowest event rates are found at the highest energies at the latest times as the energy of the supernova event reduces over time. With both the three dimensional plots it becomes apparent that whilst the first second of the supernova appears to contain the most information, there is information beyond this time from further stages. Whilst the simulation has been run for ten seconds it should be considered that a wider time period could contain further events when detecting a real supernova event. A three-dimensional Garching event plot has been plotted for a supernova at distance 50 kpc. This demonstrates the effect of distance on event rate on the time dependant Garching flux. We can still see the intial peak, and the secondary peak. Anything above 50 kpc would be difficult to see in comparison to the initial 10 kpc plot. Whilst interactions could still be measured, the peaks at the two times would be difficult to distinguish.

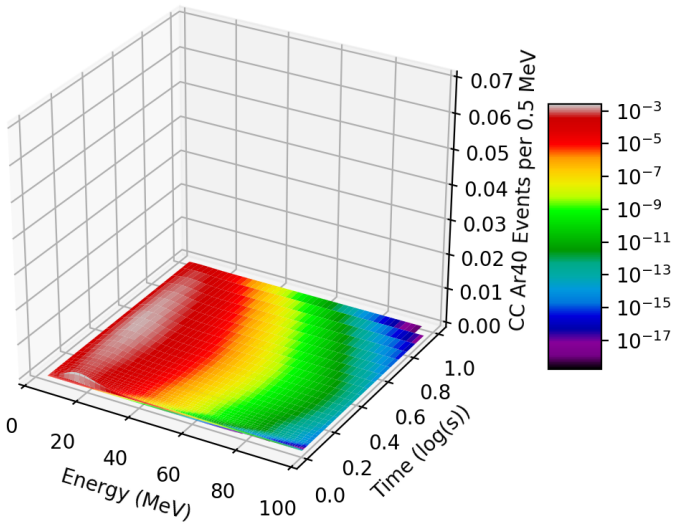

Figure 20: Three-dimensional Garching plot at distance 50 kpc.

8.6 Background Rates

There will be a naturally occuring argon isotope ^{39}Ar within a sample of argon used in detectors. This isotope will decay via beta decay

$$^{39}Ar \rightarrow {}^{39}K + \overline{\nu}_e + e^- \tag{15}$$

and will therefore release electrons and anti neutrinos into the detector. From a background rate of 1Bq/kg [52] in atmospheric argon, the assumption that this will remain approximately the same once condensed has allowed a calculation of events per second. This background event rate from within the argon is high, however will have a low energy threshold (in the order of keV) when compared to the 5 MeV used throughout this simulation. This suggests the background rate from beta decay within argon would not likely statistically impact these results. Cosmic muons could interact with liquid argon and provide events similar to the desired neutrino interactions. They could also obscure real events and make it difficult to reconstruct the neutrino events. Cosmic muons with an energy in the order of GeV would provide much longer tracks which could allow us to determine that they are not the desired interactions. These have been calculated in [53] and an error in the order of 1% has been suggested as a reasonable efficiency.

9 Conclusions

From the discussion around distance it has become apparent that in order to detect 50 events with the largest 40 ktonne detector a maximum distance of 80 kpc has been set. Anything above this distance, even with a larger volume detector, could succumb to statistical errors and background rates. For a supernova that could occur in the large magellanic cloud, just like SN1987A, a liquid argon detector of 10, 17 and 40 ktonne volumes could achieve 30±10 , 65±15 and 150±50 events respectively. These errors have been calculated from the upper and lower bounds of the distance plot created with an assumed 10% error from the Livermore and GVKM fluences. From the evidence provided in this report and evidence found in [54] it is worth noting that the Livermore fluence could be considered obsolete in the wake of GVKM and Garching models. Part of the reasoning behind this is because it does not account for flavour conversion post-bounce and therefore assumes a much larger amount of electron neutrinos from the initial infall. Whilst considering background rates it is concluded that looking for a ten second statistical change in events will likely not be affected by background rates with a supernova event at a distance closer than 50 kpc, and when compared with other detectors in the case of SNEWS would make the chances of a positive supernova signal much more likely.

Detector Volume (ktonne)	Events from Large Magellanic Cloud
10	30±10
17	65±15
40	150±50

10 References

[1] G Van Rossum. Python 2.7. 6.

[2] Wolfgang Pauli. Dear radioactive ladies and gentlemen. *Phys. Today*, 31(9):27, 1978.

[3] Enrico Fermi. An attempt of a theory of beta radiation. 1. *Z. phys*, 88(161):19, 1934.

[4] F. Reines, C. L. Cowan, F. B. Harrison, A. D. McGuire, and H. W. Kruse. Detection of the free antineutrino. *Phys. Rev.*, 117:159–173, Jan 1960.

[5] Frederick Reines and Clyde L Cowan. The neutrino. *Nature*, 178(4531):446–449, 1956.

[6] M Czakon, J Gluza, and M Zralek. Are neutrinos dirac or majorana particles? *arXiv preprint hep-ph/9910357*, 1999.

[7] W. David Arnett and Jonathan L. Rosner. Neutrino mass limits from sn1987a. *Phys. Rev. Lett.*, 58:1906–1909, May 1987.

[8] © 2015 Board of Regents of the University of Wisconsin System. `https://masterclass.icecube.wisc.edu/sites/default/files/images/neutrinos-energy.png`. Accessed 8th May 2017.

[9] Raymond Davis. A review of the homestake solar neutrino experiment. *Progress in Particle and Nuclear Physics*, 32:13 – 32, 1994.

[10] A. De Rújula, M.B. Gavela, and P. Hernández. Neutrino oscillation physics with a neutrino factory. *Nuclear Physics B*, 547(1):21 – 38, 1999.

[11] T. K. Kuo and James Pantaleone. Neutrino oscillations in matter. *Rev. Mod. Phys.*, 61:937–979, Oct 1989.

[12] QR Ahmad, RC Allen, TC Andersen, JD Anglin, G Bühler, JC Barton, EW Beier, M Bercovitch, J Bigu, S Biller, et al. Measurement of the rate of ν e+ d p+ p+ e- interactions produced by b 8 solar neutrinos at the sudbury neutrino observatory. *Physical Review Letters*, 87(7):071301, 2001.

[13] SNO. `http://www.sno.phy.queensu.ca/sno/first_results`. Accessed 8th May 2017.

[14] Massimo Turatto. Classification of supernovae. In *Supernovae and Gamma-Ray Bursters*, pages 21–36. Springer, 2003.

[15] Wolfgang Hillebrandt and Jens C Niemeyer. Type ia supernova explosion models. *Annual Review of Astronomy and Astrophysics*, 38(1):191–230, 2000.

[16] Alexei V Filippenko. Supernovae and their massive star progenitors. *arXiv preprint astro-ph/0412029*, 2004.

[17] Scott M Adams, CS Kochanek, John F Beacom, Mark R Vagins, and KZ Stanek. Observing the next galactic supernova. *The Astrophysical Journal*, 778(2):164, 2013.

[18] Swinburne University of Technology. Supernova classification tree. *http://astronomy.swin.edu.au/cosmos/S/Supernova+Classification*, Accessed 8th May 2017.

[19] `http://burro.astr.cwru.edu/Academics/Astr221/LifeCycle/highmassburn.html`. Onion-like structure of a star.

[20] Donald D Clayton. *Principles of stellar evolution and nucleosynthesis*. University of Chicago press, 1968.

[21] JM Lattimer and M Prakash. The physics of neutron stars. *Science*, 304(5670):536–542, 2004.

[22] Catalina Espinoza and Sergio Palomares-Ruiz. Detection of supernova neutrinos via coherent ν-nucleus scattering. In *Journal of Physics: Conference Series*, volume 761, page 012060. IOP Publishing, 2016.

[23] K Hirata, Takaaki Kajita, Masatoshi Koshiba, M Nakahata, Y Oyama, N Sato, A Suzuki, M Takita, Y Totsuka, T Kifune, et al. Observation of a neutrino burst from the supernova sn1987a. *Physical Review Letters*, 58(14):1490, 1987.

[24] Todd Haines, C.B. Bratton, D. Casper, A. Ciocio, R. Claus, M. Crouch, S.T. Dye, S. Errede, W. Gajewski, M. Goldhaber, T.J. Haines, T.W. Jones, D. Kielczewska, W.R. Kropp, J.G. Learned, J.M. Losecco, J. Matthews, R. Miller, M.S. Mudan, L.R. Price, F. Reines, J. Schultz, S. Seidel, E. Shumard, D. Sinclair, H.W. Sobel, L.R. Sulak, R. Svoboda, G. Thornton, and J.C. Van Der Velde. Neutrinos from sn1987a in the imb detector. *Nuclear Instruments and Methods in Physics Research Section A: Accelerators, Spectrometers, Detectors and Associated Equipment*, 264(1):28 – 31, 1988.

[25] EN Alexeyev, LN Alexeyeva, IV Krivosheina, and VI Volchenko. Detection of the neutrino signal from sn 1987a in the lmc using the inr baksan underground scintillation telescope. *Physics Letters B*, 205(2-3):209–214, 1988.

[26] Adam Burrows and James M Lattimer. Neutrinos from sn 1987a. *The Astrophysical Journal*, 318:L63–L68, 1987.

[27] C Vigorito and the Snews Working Group. Snews - the supernova early warning system. *Journal of Physics: Conference Series*, 309(1):012026, 2011.

[28] L Oberauer, F Von Feilitzsch, and W Potzel. A large liquid scintillator detector for low-energy neutrino astronomy. *Nuclear Physics B-Proceedings Supplements*, 138:108–111, 2005.

[29] S. Kubota, A. Nakamoto, T. Takahashi, T. Hamada, E. Shibamura, M. Miyajima, K. Masuda, and T. Doke. Recombination luminescence in liquid argon and in liquid xenon. *Phys. Rev. B*, 17:2762–2765, Mar 1978.

[30] M Sorel. Expected performance of an ideal liquid argon neutrino detector with enhanced sensitivity to scintillation light. *Journal of Instrumentation*, 9(10):P10002, 2014.

[31] S Fukuda, Y Fukuda, T Hayakawa, E Ichihara, M Ishitsuka, Y Itow, T Kajita, J Kameda, K Kaneyuki, S Kasuga, et al. The super-kamiokande detector. *Nuclear Instruments and Methods in Physics Research Section A: Accelerators, Spectrometers, Detectors and Associated Equipment*, 501(2):418–462, 2003.

[32] J Boger, R.L Hahn, J.K Rowley, A.L Carter, B Hollebone, D Kessler, I Blevis, F Dalnoki-Veress, A DeKok, J Farine, D.R Grant, C.K Hargrove, G Laberge, I Levine, K McFarlane, H Mes, A.T Noble, V.M Novikov, M O'Neill, M Shatkay, C Shewchuk, D Sinclair, E.T.H Clifford, R Deal, E.D Earle, E Gaudette, G Milton, B Sur, J Bigu, J.H.M Cowan, D.L Cluff, E.D Hallman, R.U Haq, J Hewett, J.G Hykawy, G Jonkmans, R Michaud, A Roberge, J Roberts, E Saettler, M.H Schwendener, H Seifert, D Sweezey, R Tafirout, C.J Virtue, D.N Beck, Y.D Chan, X Chen, M.R Dragowsky, F.W Dycus, J Gonzalez, M.C.P Isaac, Y Kajiyama, G.W Koehler, K.T Lesko, M.C Moebus, E.B Norman, C.E Okada, A.W.P Poon, P Purgalis, A Schuelke, A.R Smith, R.G Stokstad, S Turner, I Zlimen, J.M Anaya, T.J Bowles, S.J Brice, Ernst-Ingo Esch, M.M Fowler, Azriel Goldschmidt, A Hime, A.F McGirt, G.G Miller, W.A Teasdale, J.B Wilhelmy, J.M Wouters, J.D Anglin, M Bercovitch, W.F Davidson, R.S Storey, S Biller, R.A Black, R.J Boardman, M.G Bowler, J Cameron, B Cleveland, A.P Ferraris, G Doucas, H Heron, C Howard, N.A Jelley, A.B Knox, M Lay, W Locke, J Lyon, S Majerus, M Moorhead, M Omori, N.W Tanner, R.K Taplin, M Thorman, D.L Wark, N West, J.C Barton, P.T Trent, R Kouzes, M.M Lowry, A.L Bell, E Bonvin, M Boulay, M Dayon, F Duncan, L.S Erhardt, H.C Evans, G.T Ewan, R Ford, A Hallin, A Hamer, P.M Hart, P.J Harvey, D Haslip, C.A.W Hearns, R Heaton, J.D Hepburn, C.J Jillings, E.P Korpach, H.W Lee, J.R Leslie, M.-Q Liu, H.B Mak, A.B McDonald, J.D MacArthur, W McLatchie, B.A Moffat, S Noel, T.J Radcliffe, B.C Robertson, P Skensved, R.L Stevenson, X Zhu, S Gil, J Heise, R.L Helmer, R.J Komar, C.W Nally, H.S Ng, C.E Waltham, R.C Allen, G Bühler, H.H Chen, G Aardsma, T Andersen, K Cameron, M.C Chon, R.H Hanson, P Jagam, J Karn, J Law, R.W Ollerhead, J.J Simpson, N Tagg, J.-X Wang, C Alexander, E.W Beier, J.C Cook, D.F Cowen, E.D Frank, W Frati, P.T

Keener, J.R Klein, G Mayers, D.S McDonald, M.S Neubauer, F.M Newcomer, R.J Pearce, R.G.Van de Water, R.Van Berg, P Wittich, Q.R Ahmad, J.M Beck, M.C Browne, T.H Burritt, P.J Doe, C.A Duba, S.R Elliott, J.E Franklin, J.V Germani, P Green, A.A Hamian, K.M Heeger, M Howe, R.Meijer Drees, A Myers, R.G.H Robertson, M.W.E Smith, T.D Steiger, T.Van Wechel, and J.F Wilkerson. The sudbury neutrino observatory. *Nuclear Instruments and Methods in Physics Research Section A: Accelerators, Spectrometers, Detectors and Associated Equipment*, 449(1–2):172 – 207, 2000.

[33] C. Kraus. {SNO} with liquid scintillator: Sno+. *Progress in Particle and Nuclear Physics*, 57(1):150 – 152, 2006. International Workshop of Nuclear Physics 27th courseNeutrinos in Cosmology, in Astro, Particle and Nuclear PhysicsEttore Majorana Center for Scientific Culture.

[34] J Hartnell and the Sno+ collaboration. Neutrinoless double beta decay with sno+. *Journal of Physics: Conference Series*, 375(4):042015, 2012.

[35] S Andringa, E Arushanova, S Asahi, M Askins, DJ Auty, AR Back, Z Barnard, N Barros, EW Beier, A Bialek, et al. Current status and future prospects of the sno. *Advances in High Energy Physics*, 2016, 2016.

[36] RE Latimer. Distillation of air. *Chemical Engineering Progress*, 63(2):35, 1967.

[37] P Cennini, S Cittolin, L Dumps, A Placci, JP Revol, C Rubbia, L Fortson, P Picchi, F Cavanna, G Piano Mortari, et al. Argon purification in the liquid phase. *Nuclear Instruments and Methods in Physics Research Section A: Accelerators, Spectrometers, Detectors and Associated Equipment*, 333(2-3):567–570, 1993.

[38] Oxisorb is a trademark of messer griesheim gmbh. Filed: 1972-05-22.

[39] B Rebel, M Adamowski, W Jaskierny, H Jostlein, C Kendziora, R Plunkett, S Pordes, R Schmitt, T Tope, and T Yang. Results from the fermilab materials test stand and status of the liquid argon purity demonstrator. In *Journal of Physics: Conference Series*, volume 308, page 012023. IOP Publishing, 2011.

[40] C Rubbia, M Antonello, P Aprili, B Baibussinov, M Baldo Ceolin, L Barze, P Benetti, E Calligarich, N Canci, F Carbonara, et al. Underground operation of the icarus t600 lar-tpc: first results. *Journal of Instrumentation*, 6(07):P07011, 2011.

[41] R Acciarri, MA Acero, M Adamowski, C Adams, P Adamson, S Adhikari, Z Ahmad, CH Albright, T Alion, E Amador, et al. Long-baseline neutrino facility (lbnf) and deep underground neutrino experiment (dune) conceptual design report, volume 4 the dune detectors at lbnf. *arXiv preprint arXiv:1601.02984*, 2016.

[42] DUNE. Dune website. *http://www.dunescience.org/wp-content/uploads/2016/12/LBNE_Graphic_061615_2016.jpg*, Accessed 8th May 2017.

[43] Alex Beck, Farzan Beroz, Rachel Carr, Huaiyu Duan, Alex Friedland, Nicolas Kaiser, Jim Kneller, Alexander Moss, Diane Reitzner, Kate Scholberg, et al. Snowglobes: Supernova observatories with globes.

[44] Patrick Huber, Manfred Lindner, and Walter Winter. Simulation of long-baseline neutrino oscillation experiments with globes:(general long baseline experiment simulator). *Computer Physics Communications*, 167(3):195–202, 2005.

[45] Jerome Gava, James Kneller, Cristina Volpe, and GC McLaughlin. Dynamical collective calculation of supernova neutrino signals. *Physical review letters*, 103(7):071101, 2009.

[46] T Totani, K Sato, HE Dalhed, and JR Wilson. Future detection of supernova neutrino burst and explosion mechanism. *The Astrophysical Journal*, 496(1):216, 1998.

[47] I Gil-Botella and André Rubbia. Decoupling supernova and neutrino oscillation physics with lar tpc detectors. *Journal of Cosmology and Astroparticle Physics*, 2004(08):001, 2004.

[48] E Kolbe, Karlheinz Langanke, G Martinez-Pinedo, and P Vogel. Neutrino–nucleus reactions and nuclear structure. *Journal of Physics G: Nuclear and Particle Physics*, 29(11):2569, 2003.

[49] A Mirizzi, G G Raffelt, and P D Serpico. Earth matter effects in supernova neutrinos: optimal detector locations. *Journal of Cosmology and Astroparticle Physics*, 2006(05):012, 2006.

[50] Georg G Raffelt, Mathias Th Keil, Robert Buras, Hans-Thomas Janka, and Markus Rampp. Supernova neutrinos: Flavor-dependent fluxes and spectra, 2003.

[51] Rene Brun and Fons Rademakers. Rootóan object oriented data analysis framework. *Nuclear Instruments and Methods in Physics Research Section A: Accelerators, Spectrometers, Detectors and Associated Equipment*, 389(1-2):81–86, 1997.

[52] Henning O Back, F Calaprice, C Condon, E de Haas, R Ford, C Galbiati, Augusto Goretti, T Hohman, An Inanni, B Loer, et al. First large scale production of low radioactivity argon from underground sources. *arXiv preprint arXiv:1204.6024*, 2012.

[53] David Gerstle and Stephen Pordes. Cosmic ray rates on a surface liquid argon tpc. *LBNE-doc-5950 (August 2006)*, 2006.

[54] V Fischer, T Chirac, T Lasserre, C Volpe, M Cribier, M Durero, J Gaffiot, T Houdy, A Letourneau, G Mention, et al. Prompt directional detection of galactic supernova by combining large liquid scintillator neutrino detectors. *Journal of Cosmology and Astroparticle Physics*, 2015(08):032, 2015.

11 Appendix

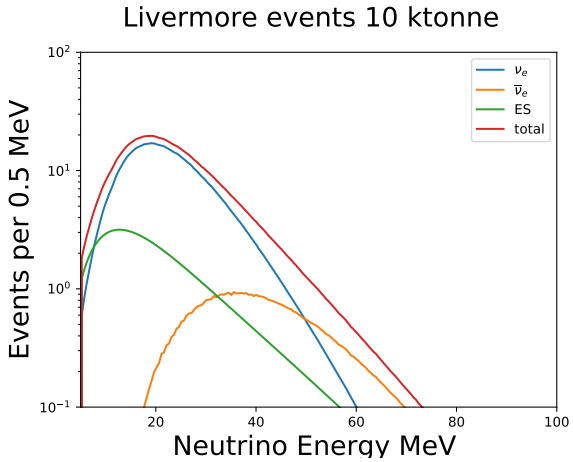

Figure 21: A plot of Events against neutrino energy for a 10 ktonne Liquid Argon TPC with the Livermore fluence.

Event	Events Livermore 10 ktonne
$\nu_e + {}^{40}Ar \rightarrow e^- + {}^{40}K^*$	672
$\overline{\nu}_e + {}^{40}Ar \rightarrow e^+ + {}^{40}Cl^*$	56
$\nu_x + e^- \rightarrow \nu_x + e^-$	134
Total	942

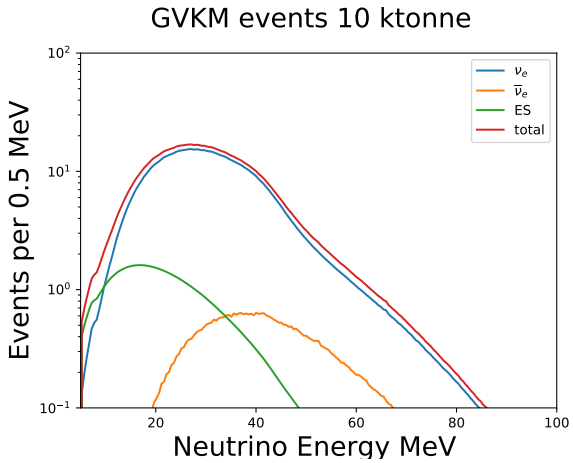

Figure 22: A plot of Events against neutrino energy for a 10 ktonne Liquid Argon TPC with the GVKM fluence.

Event	Events GVKM 10 ktonne
$\nu_e + {}^{40}Ar \rightarrow e^- + {}^{40}K^*$	828
$\overline{\nu}_e + {}^{40}Ar \rightarrow e^+ + {}^{40}Cl^*$	39
$\nu_x + e^- \rightarrow \nu_x + e^-$	75
Total	942

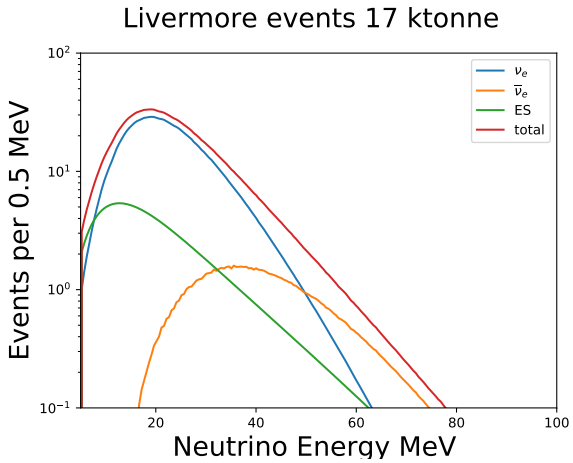

Figure 23: A plot of Events against neutrino energy for a 17 ktonne Liquid Argon TPC with the Livermore fluence.

Event	Events Livermore 17 ktonne
$\nu_e + {}^{40}Ar \rightarrow e^- + {}^{40}K^*$	1142
$\overline{\nu}_e + {}^{40}Ar \rightarrow e^+ + {}^{40}Cl^*$	95
$\nu_x + e^- \rightarrow \nu_x + e^-$	230
Total	1467

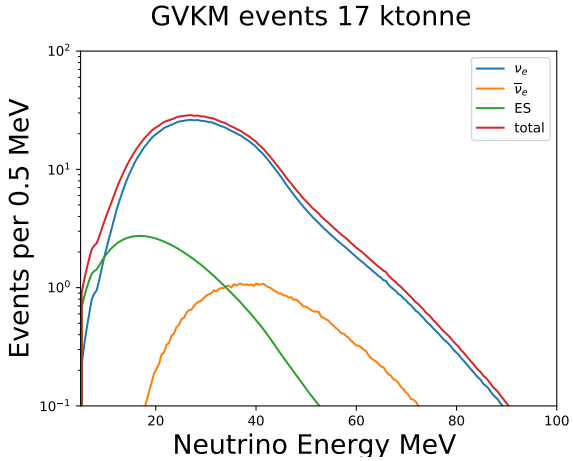

Figure 24: A plot of Events against neutrino energy for a 17 ktonne Liquid Argon TPC with the GVKM fluence.

Event	Events GVKM 17 ktonne
$\nu_e + {}^{40}Ar \rightarrow e^- + {}^{40}K^*$	1408
$\overline{\nu}_e + {}^{40}Ar \rightarrow e^+ + {}^{40}Cl^*$	66
$\nu_x + e^- \rightarrow \nu_x + e^-$	127
Total	1601

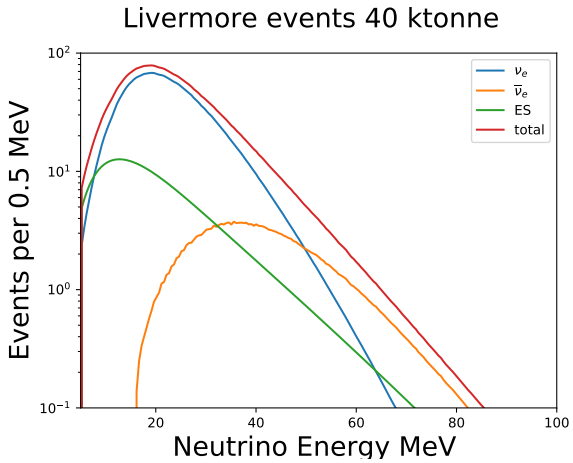

Figure 25: A plot of Events against neutrino energy for a 40 ktonne Liquid Argon TPC with the Livermore fluence.

Event	Events Livermore 40 ktonne
$\nu_e + {}^{40}Ar \rightarrow e^- + {}^{40}K^*$	2688
$\overline{\nu}_e + {}^{40}Ar \rightarrow e^+ + {}^{40}Cl^*$	225
$\nu_x + e^- \rightarrow \nu_x + e^-$	546
Total	3459

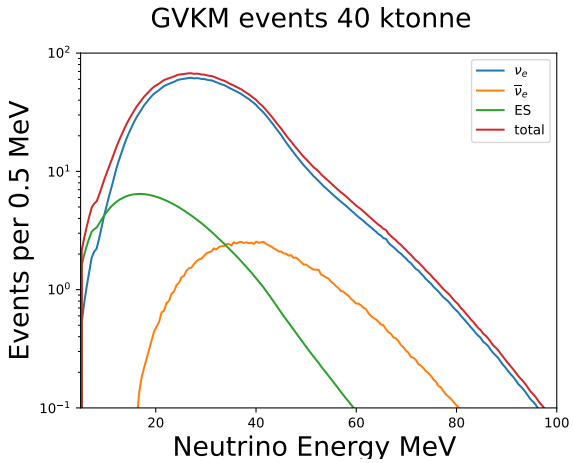

Figure 26: A plot of events against neutrino energy for a 40 ktonne Liquid Argon TPC with the GVKM fluence.

Event	Events GVKM 40kton
$\nu_e + {}^{40}Ar \rightarrow e^- + {}^{40}K^*$	3314
$\overline{\nu}_e + {}^{40}Ar \rightarrow e^+ + {}^{40}Cl^*$	156
$\nu_x + e^- \rightarrow \nu_x + e^-$	308
Total	3778

The following code was created and used by myself to plot the GVKM fluence as provided in the SNOwGLoBES software package.

```
import matplotlib.pyplot as plt
import pylab as pylab
import numpy as np
x, y1, y2, y3, y4, y5, y6 = np.loadtxt('gvkm.dat', unpack
    =True)
#Unpacked 7 data columns as different variables
fig = plt.figure()
#Changing from GeV to MeV
newx = x*(1000)
plt.plot(newx,y1, label=r'$\nu_e$',linewidth=3)
plt.plot(newx,y4, label=r'$\overline{\nu}_e$',linewidth
    =3)
y7 = np.add(y2, y3)
y8 = np.add(y5, y6)
y9 = np.add(y7, y8)
plt.plot(newx,y9, label=r'$\nu_x + \overline{\nu}_x$',
    linewidth=2)
fig.suptitle('GVKM ', fontsize=12)
plt.xlabel('Neutrino Energy MeV ', fontsize=12)
plt.ylabel('Neutrinos per 0.2 MeV per cm$^2$', fontsize
    =12)
plt.xlim([0,100])
plt.ylim([0,4500e6])
plt.legend(fontsize=10)
fig.savefig('GVKMnewunits.pdf')
plt.show()
```

The following code was created and used by myself to plot the Livermore fluence as provided in the SNOwGLoBES software package.

```
import matplotlib.pyplot as plt
import pylab
import numpy as np
x, y1, y2, y3, y4, y5, y6 = np.loadtxt('livermore.dat',
    unpack=True)
#Unpacked 7 data columns as different variables
fig = plt.figure()
#Changing from GeV to MeV
newx = x*(1000)
plt.plot(newx,y1, label=r'$\nu_e$', linewidth=3)
plt.plot(newx,y4, label=r'$\overline{\nu}_e$', linewidth
    =3)
y7 = np.add(y2, y3)
y8 = np.add(y5, y6)
y9 = np.add(y7, y8)
plt.plot(newx,y9, label=r'$\nu_x + \overline{\nu}_x$',
    linewidth=2)
fig.suptitle('LIVERMORE', fontsize=12)
plt.xlabel('Neutrino Energy MeV ', fontsize=12)
plt.ylabel('Neutrinos per 0.2 MeV per cm$^2$', fontsize
    =12)
pylab.xlim([0,100])
pylab.ylim([0,4500e6])
plt.legend(fontsize=10)
fig.savefig('LIVERMOREnewunits.pdf')
plt.show()
```

The following code was created and used by myself to plot the Argon cross sections as provided in the SNOwGLoBES software package.

```
import matplotlib.pyplot as plt
import pylab
import numpy as np
x, y1, y2, y3, y4, y5, y6 = np.loadtxt('xs_numu_e.dat',
    unpack=True)
x2, a1, a2, a3, a4, a5, a6 = np.loadtxt('xs_nue_Ar40.dat
    ', unpack=True)
x3, b1, b2, b3, b4, b5, b6 = np.loadtxt('
    xs_nuebar_Ar40edited.dat', unpack=True)
fig = plt.figure()
\#Converting from log
GEVx3=(10**x3)
GEVx = (10**x)
GEVx2 = (10**x2)
\#Converting to MeV
MEVx = GEVx*1000
MEVx2 = GEVx2*1000
MEVx3 = GEVx3*1000
y7 = np.add(y2, y3)*GEVx/2
y8 = np.add(y5, y6)*GEVx/2


plt.plot(MEVx,y1*GEVx,'k:', label=r'$\nu_e$', linewidth
    =2)
plt.plot(MEVx,y4*GEVx,'k-', label=r'$\overline{\nu}_e$',
    linewidth=2)
plt.plot(MEVx,y7, 'k--', label=r'$\nu_x$', linewidth=2)
plt.plot(MEVx,y8, 'k-.', label=r'$\overline{\nu}_x$',
    linewidth=2)
plt.plot(MEVx3,b4*GEVx3, label=r'$\overline{\nu}_e$ -
    Ar40', linewidth=2)
plt.plot(MEVx2,a1*GEVx2,  label=r'$\nu_e$ - Ar40',
    linewidth=2)
fig.suptitle('Cross Sections', fontsize=15)
plt.xlabel('Neutrino Energy MeV ', fontsize=15)
plt.ylabel('Cross Sections $10^{-38}$ cm$^2$', fontsize
    =15)
plt.yscale('log')
plt.xlim([5,100])
plt.ylim([0.0000001,100])
plt.legend(loc = 'upper left',ncol=3, fontsize=15)
fig.savefig('crosssections.jpg')
plt.show()
```

The following code was created and used by myself to create a three dimensional plot for the Garching fluence.

```
from mpl_toolkits.mplot3d import Axes3D
from matplotlib import cm, ticker
import matplotlib.pyplot as plt
from matplotlib.mlab import griddata
from matplotlib.collections import LineCollection
import numpy as np
from math import log
from matplotlib.colors import LogNorm

fig = plt.figure()
ax = fig.gca(projection='3d')

z = np.genfromtxt('yvalues.txt', unpack=True) #CC


#unpacking 3 columns from key file
t1, t2, t3 = np.genfromtxt('/Users/samuelnorthwood/
    snowglobes-dev/garching_pinched_info_key.dat',
    delimiter=' ', unpack=True)

fig = plt.figure()

p,q = np.genfromtxt('/Users/samuelnorthwood/out/
    pinched_0_nue_Ar40_ar17kt_events_smeared.dat',
    delimiter=' ', skip_footer=2, unpack=True)

p = p*1000

t4 = t2 -t2[0]+1
t5 = np.log10(t4)

z1 = np.log10(z+1)



X,Y = np.meshgrid(p,t5)

Z = z1.reshape((300,200))

print(X.shape)
```

```
print(Y.shape)
print(Z.shape)


fig = plt.figure()
ax = fig.gca(projection='3d')

surf = ax.plot_surface(X, Y, Z, cmap=cm.nipy_spectral,
    norm = LogNorm())
ax.set_xlabel('Energy (MeV)')
ax.set_zlabel(' CC Ar40 Events per 0.5 MeV')
ax.set_ylabel('Time (log(s))')
ax.set_xlim(0, 100)
plt.axhline(y=2*10^-2, color='k', linestyle='-',
    linewidth=100)


fig.colorbar(surf, shrink=0.5, aspect=5)



plt.show()
```

The following code was created and used by myself for a distance against events plot from the Livermore and GVKM eventrates.

```
from __future__ import division
from mpl_toolkits.mplot3d import Axes3D
from matplotlib import cm, ticker
import matplotlib.pyplot as plt
from matplotlib.mlab import griddata
import numpy as np
from math import log
from matplotlib.colors import LogNorm


fig = plt.figure()


#10kton
events10livermore= 807*0.9
events10GVKM = 916*1.1
newevents10livermore = 807*100/10000*0.9
newevents10GVKM = 916*100/10000*1.1
Xevents10livermore = 807*100*0.9
Xevents10GVKM = 916*100*1.1
Xnewevents10livermore = 807/10000*0.9
Xnewevents10GVKM = 916/10000*1.1
#17kton
events17livermore= 1376*0.9
events17GVKM = 1558*1.1
newevents17livermore= 1376*100/10000*0.9
newevents17GVKM = 1558*100/10000*1.1
Xevents17livermore= 1376*100*0.9
Xevents17GVKM = 1558*100*1.1
Xnewevents17livermore = 1376/10000*0.9
Xnewevents17GVKM = 1558/10000*1.1
#40kton
events40livermore= 3243*0.9
events40GVKM = 3672*1.1
newevents40livermore= 3243*100/10000*0.9
newevents40GVKM = 3672*100/10000*1.1
Xevents40livermore= 3243*100*0.9
Xevents40GVKM = 3672*100*1.1
Xnewevents40livermore = 3243/10000*0.9
Xnewevents40GVKM = 3672/10000*1.1
```

```
x = (1,10,100,1000)
y = (Xevents10livermore, events10livermore,
    newevents10livermore, Xnewevents10livermore)
z = (Xevents10GVKM,events10GVKM, newevents10GVKM,
    Xnewevents10GVKM)
p = (Xevents17livermore,events17livermore,
    newevents17livermore, Xnewevents17livermore)
q = (Xevents17GVKM, events17GVKM, newevents17GVKM,
    Xnewevents17GVKM)
r = (Xevents40livermore, events40livermore,
    newevents40livermore, Xnewevents40livermore)
s = (Xevents40GVKM, events40GVKM, newevents40GVKM,
    Xnewevents40GVKM)

print(x)
print(y)
print(z)
print(q)
print(p)
print(r)
print(s)

plt.loglog(x,y, 'c', label = '10kton')
plt.loglog(x,z, 'c')
plt.loglog(x,p, 'r', label = '17kton')
plt.loglog(x,q, 'r')
plt.loglog(x,r, 'orange', label = '40kton')
plt.loglog(x,s, 'orange')
plt.xlim(1,1000)
plt.xlabel('Distance to Supernovae (kpc)')
plt.ylabel('Total Neutrino Events')


plt.axvline(x=10, color='green', linestyle='-', ymax=1.2,
     linewidth=1)
plt.axvline(x=48.5, color='green', linestyle='-',
    linewidth=1)
plt.axvline(x=780, color='green', linestyle='-',
    linewidth=1)
plt.axhline(y=100, color='k', linestyle='--')
plt.axhline(y=50, color='gray', linestyle='--')
plt.axvline(x=np.sqrt(807), ymax=0.47, color='k',
    linestyle='--')
plt.text(np.sqrt(807),0.02,'28',fontsize=9)
plt.axvline(x=np.sqrt(1376), ymax=0.47,color='k',
    linestyle='--')
```

```
plt.text(np.sqrt(1376),0.02,'37',fontsize=9)
plt.axvline(x=np.sqrt(3243), ymax=0.47,color='k',
    linestyle='--')
plt.text(np.sqrt(3243),0.02,'57',fontsize=9)
plt.axvline(x=np.sqrt(2*807), ymin=0.435, color='gray',
    linestyle='--')
plt.text(np.sqrt(2*807),760000,'40',fontsize=9)
plt.axvline(x=np.sqrt(2*1376), ymin=0.435,color='gray',
    linestyle='--')
plt.text(np.sqrt(2*1376),760000,'52',fontsize=9)
plt.axvline(x=np.sqrt(2*3243), ymin=0.435,color='gray',
    linestyle='--')
plt.text(np.sqrt(2*3243),760000,'80',fontsize=9)
plt.text(1,50,'50 events',fontsize=9)
plt.text(1,100,'100 events',fontsize=9)
plt.text(4, 6500000, 'Simulation Distance',rotation=20,
    fontsize=9)
plt.text(20, 6500000, 'Large Magellanic Cloud',rotation
    =20, fontsize=9)
plt.text(400, 4500000, 'Andromeda', rotation=20, fontsize
    =9)
plt.legend(loc='lower left')
plt.show()
plt.savefig('distance.pdf')
```